# SUBGRIDDING TECHNIQUE FOR THE GEODESIC FDTD ALGORITHM

**Y. Wang and Q. Cao**

College of Information Science and Technology
Nanjing University of Aeronautics and Astronautics
29, Yudao Street, Nanjing, China

**Abstract**—This work presents a two-dimensional (2D) subgrid technique for the geodesic finite different time-domain (FDTD) algorithm, which is applied to solve global extremely low frequency (ELF) electromagnetic (EM) wave propagation problems in the Earth-ionosphere system. The new technology provides arbitrarily locale resolution to study finer structure without disturb the global grid structure. Combined with the subgrid technique, the new geodesic FDTD algorithm can solve EM propagation problems in specific locale regions without extra computational burden. Based on the original geodesic FDTD formulations, the 2D subgrid technique is developed, and its computational stable relation is derived and analyzed. Then, possible three-dimensional (3D) subgrid structure is proposed. Finally, potential applications for the subgrid technique are suggested.

## 1. INTRODUCTION

Propagation of extremely low frequency EM waves in the Earth-ionosphere is an interesting and important investigation area in the last few decades, and it has applied in many fields related to the Earth science and other fields. As reported in [1], "Currently, propagation phenomena below 300 kHz form the physics basis of remote-sensing investigations of lightning and sprites, global temperature change, subsurface structures, submarine communications, and potential Earthquake precursors".

Solutions to the ELF EM wave propagation problems has been focused on analytical formulations [2]. Recently, using the time domain

algorithm to simulate the wave propagation in the Earth-ionosphere system is becoming a hot topic [1, 3–6]. The review by Simpson [1] has provided a brief introduction to the relative works in this field.

In 2004, Simpson and Taflove proposed a novel 2D geodesic FDTD grid model [7], in which the grid was comprised entirely of hexagonal cells except for 12 pentagonal cells needed for grid completion. After that, they also extended this 2D grid into a fully 3-D space lattice [8, 9]. This geodesic FDTD method is superior to the previous widely-used latitude-longitude FDTD method [5, 6, 10–12] because it has provided much more numerically isotropic wave propagation, and completely has avoided grid-cell convergences at the Earth's poles [1].

Both the latitude-longitude and geodesic FDTD algorithms of the Earth-ionosphere system focus on solving global ELF EM propagation problems. However in most applications, the EM fields in specific local regions are more preferable than those in other regions. To achieve this goal, higher resolution is required in specific local regions when modeling the Earth-ionosphere system. It is obvious that if the regions located outside interested areas are simulated using the same high resolution then unnecessary expenditure of computer resources are increased. In order to solve this problem, it is considered only to model the locale region in the Earth-ionosphere system using the traditional FDTD algorithm [3, 4]. However, solving EM problems in this way will lose global influence on locale regions, thus giving inaccurate solutions. In fact, this method can only deal EM problems with spectrum higher than ELF, because the global influence on locale regions can be ignored for EM wave with spectrum higher than ELF due to the fast attenuation rate [13, 14]. In fact, the direct way to study locale ELF propagation problems coupled with global influence is to only increase the resolution of the interested areas. Several techniques applied in other algorithms have the potential possibilities to solve this problem [12, 15, 16]. The subgrid techniques introduced in [15] is the general approach for these problems, and it focused only on the Cartesian subgrids. From 2002, Simpson and Taflove [7, 12] proposed a technique to reduce the eccentricity of the cells in the polar regions by merging adjacent grid-cells in the East-West direction. This technology has been pointed out the possibility to divide grid-cell into subgrids in the spherical FDTD model. In [16], a local high-resolution technique was proposed based on a different technique, but it was only effective for the latitude-longitude FDTD algorithm and with many limitations.

In this paper, we report a subgrid technology in the geodesic FDTD algorithm for the purpose of increasing local resolution when simulating Earth-ionosphere system. In this new algorithm, specific triangular grid cell of the geodesic FDTD model is divided into four

smaller triangular grid cells in order to achieve higher resolution. Based on this algorithm, the local EM field can be obtained with higher accuracy and lower computational cost. The rest of the paper is organized as follows. In Section 2, the basic idea of the geodesic FDTD algorithm is briefly reviewed. Then, we introduced the details of the subgridding method in Section 3. An example of using the subgridding method in the geodesic is described in Section 4. After that, several potential applications for the subgrid technique are proposed. Finally, we conclude our work.

## 2. THE GEODESIC FDTD ALGORITHM

The geodesic FDTD grid method is initially proposed by Simpson and Taflove [7, 8] to simulate the ELF EM wave propagation problems in the Earth-ionosphere system. Our previous works have verified the efficiency of this algorithm in solving the global EM problems [14, 17]. The basic idea of this FDTD grid technique is to model the entire Earth-ionosphere system using the alternating planes of the transverse-magnetic (TM) and the transverse-electric (TE) field components, which are comprised of triangular grid-cells or hexagonal grid-cells (including 12 pentagonal grid-cells), separately. Figure 1 presents a typical geodesic grid model, in which the triangular grid cells and the hexagon grid cells are illustrated using different lifestyles. Note that the radial projections of the vertexes of the hexagonal grid-cells (or pentagonal grid-cells) on the triangular combined plane are the circumcenters of the triangular grid cells. Based on this model, the
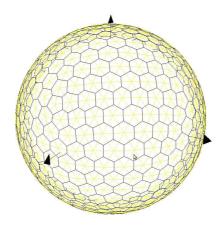


**Figure 1.** The 3D geodesic FDTD model.

integral form of Ampere's Law and Faraday's Law are applied to
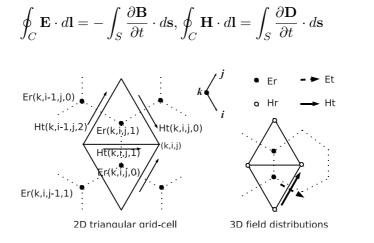develop the FDTD time-stepping relations:

$$\oint_C \mathbf{E} \cdot d\mathbf{l} = -\int_S \frac{\partial \mathbf{B}}{\partial t} \cdot d\mathbf{s}, \oint_C \mathbf{H} \cdot d\mathbf{l} = \int_S \frac{\partial \mathbf{D}}{\partial t} \cdot d\mathbf{s} \qquad (1)$$



**Figure 2.** The 2D triangular grid-cell and 3D field distributions of
the geodesic FDTD algorithm.

Figure 2 is plotted to show the details of a triangular FDTD grid-
cell. In the figure, $i$ and $j$ stand for the directions in the tangential
(horizontal) plane; $k$ is the radial (vertical) direction. Update equation,
for the up grid-cell is as the follow, only Er component,

$$Er^{n+1}(k,i,j,1) = Er^n(k,i,j,1) + \frac{\Delta t}{\varepsilon \Delta S(k,i,j,1)}$$
$$\times \{Ht^{n+0.5}(k,i,j,1) \times \Delta l_1(k,i,j,1) - Ht^{n+0.5}(k,i,j,0) \times \Delta l_2(k,i,j,1)$$
$$-Ht^{n+0.5}(k,i-1,j,2) \times \Delta l_0(k,i,j,1)\} \qquad (2)$$

where $\Delta t$, $\Delta l_x$ and $\Delta S$ are the time-step, the $x$th wall length of the
triangular grid-cell and the area of the cell, respectively.

The 2D FDTD time-stepping algorithm is completed by specifying
the update equations for the magnetic field. For example, referring to
the tangential magnetic field quantities $Ht$ in the up triangular grid
cells shown in Figure 3, we have

$$Ht^{n+1.5}(k,i-1,j,2) = Ht^{n+0.5}(k,i-1,j,2) + \frac{\Delta t}{\mu \delta_t(k,i-1,j,2)}$$
$$\times \{Er^{n+1}(k,i-1,j,0) - Er^{n+1}(k,i,j,1)\} \quad (3)$$
$$Ht^{n+1.5}(k,i,j,1) = Ht^{n+0.5}(k,i,j,1) + \frac{\Delta t}{\mu \delta_t(k,i,j,1)}$$
$$\times \{Er^{n+1}(k,i,j,1) - Er^{n+1}(k,i,j,0)\} \qquad (4)$$

$$Ht^{n+1.5}(k,i,j,0) = Ht^{n+0.5}(k,i,j,0) + \frac{\Delta t}{\mu \delta_t(k,i,j,0)}$$
$$\times \{Er^{n+1}(k,i,j+1,0) - Er^{n+1}(k,i,j,1)\} \quad (5)$$

where $\delta$ is the distance between adjacent $Er$'s at $Ht$.

For field components $Et$ and $Hr$, the updated equations are similarly,

$$Hr^{n+1.5} = Hr^{n+0.5} + \frac{\Delta t}{\mu \Delta S_{hexagon}} \times \sum (Et^{n+1} \times \delta_t) \quad (6)$$

$$Et^{n+1} = Et^n + \frac{\Delta t}{\varepsilon \Delta_l} \times \sum Hr^{n+0.5} + \frac{\Delta t}{\varepsilon \delta_r} \times \sum Ht^{n+0.5} \quad (7)$$

where $\delta t$ is the distance between adjacent $Et$'s at $Ht$ (radial direction). It is noted that in 3D update equations, when updating $Ht$, the radial field quantity $Et$ is added into the update equations.

## 3. THE 2D SUBGRID TECHNOLOGY

Figure 3 is illustrated the geometry of the subgrid technology for the TM planes in the Earth-ionosphere model. The main idea of this algorithm is to divide the triangular grid-cell into four smaller grid-cells in order to increase the resolution of specific regions in the global model and so on. In Figure 3, the triangular grid in the TM plane is divided into 4 smaller subgrids, the division is completed by connecting the middle points of the triangular grid-cells edges. In the figure, the $E$ and $H$ denote fields in the primary grid, and $e$ and $h$ denote fields in the subgrid.

According to the subgrid geometry structure shown in Figure 3, the field quantities in the subgrid cells ($er$, $ht$) have to be calculated to complete the FDTD algorithm, also a special treatment is needed for border field quantities of the subgrid cells.

First, referring to the subgrid cells in Figure 3, we have

$$er^{n+1} = er^n + \frac{\Delta t}{\varepsilon \Delta S_{sub}} \times \sum (ht^{n+0.5} \times \Delta l_{sub}) \quad (8)$$

where $\Delta t$, $\Delta S_{sub}$ and $\Delta l_{sub}$ are the time-step, the area and the wall length of the subgrid cell centered around $er$, respectively.

The update equations for the border field quantities $Er$ are

$$Er^{n+1} = Er^n + \frac{\Delta t}{\varepsilon \Delta S_{norm}} \times$$
$$\left\{ \sum (Ht^{n+0.5} \times \Delta l_{norm}) + \sum (ht^{n+0.5} \times \Delta l_{sub}) \right\} \quad (9)$$
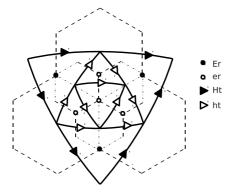
**Figure 3.** Subgrid technologies for triangular grid-cell, the original triangle in the middle is divided into four smaller sub triangles.
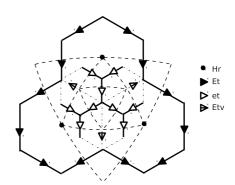
**Figure 4.** The possible subgrid technique for hexagonal grid-cell, virtual field quantities (Etv) are added to form completely FDTD algorithm.

where $\Delta S_{norm}$ and $\Delta l_{norm}$ are the area and the wall length of the normal cell centered around $Er$, respectively. Other the radial electric field quantities can be updated using normal geodesic FDTD algorithm.

For the tangential magnetic field $ht$ inside grid-cell that is subgridded, we have

$$ht^{n+1.5} = ht^{n+0.5} + \frac{\Delta t}{\mu \delta_{t,sub}} \times \sum er^{n+1} \qquad (10)$$

where $\delta_{t,sub}$ is the distance between adjacent $er$'s at $ht$, and $\delta_r$ is the distance between adjacent TE planes.

To calculate the $ht$ field quantities in the edge of the subgrid cells, we assume that the field quantities inside the normal grid-cells are distributed evenly, and obtain the approximation update equation

$$ht^{n+1.5} \approx ht^{n+0.5} + \frac{\Delta t}{\mu \delta_{t,sub}} \times \left( er^{n+1} \pm Er^{n+1}_{border} \right) \qquad (11)$$

where $Er^{n+1}_{border}$ stands for the average field quantity in the normal grid-cell in the subgrid border.

Note that the stable relation is decided by the smallest grid-cell distance in the geodesic model. Here we consider the smallest triangular grid-cell (subgrid cell) is regular triangles, and use the approximate stable relation

$$C\Delta t \le \frac{\sqrt{3}}{2} \Delta l_{sub,min} \qquad (12)$$

where $C$ is the light speed, $\Delta l_{sub,min}$ is the minimum wall length of the subgrid cells.

To complete the 3D subgrid technology of the geodesic FDTD algorithm, the corresponding grid-cell divisions have to be made for the hexagon grid-cells in the TE plane. Possible subgrid cell structure is illustrated in Figure 4. In the figure, the virtual field quantities ($Etv$) are needed for information transfer between the normal grid-cell and the subgrid cell. The update equations for the 3D subgrid technique are to be developed in further work.

## 4. VALIDATIONS

In order to validate the subgrid technique for the geodesic FDTD algorithm, a Gaussian pulse is excited at the equator, and monitored in the antipode. Figure 5 presents the simulation results of wave propagation in the Earth's sphere ($dt = 3.0 \times 10^{-5}$ s). To obtain the results in the figure, three different simulation conditions are introduced: A) order 6th geodesic FDTD algorithm (top result), B) order 5th geodesic FDTD algorithm with subgrid technique (middle result), C) order 5th geodesic FDTD algorithm (bottom result). The results are similar to each other (sources are the same)and indicate a
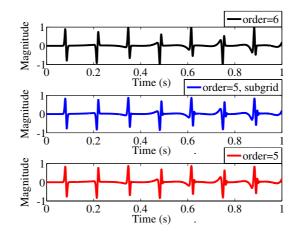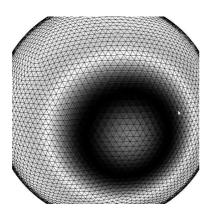


**Figure 5.** ELF wave propagation validation. A source is placed in a normal grid-cell and observed in the antipode of the sphere under different simualtion conditions. Top: simulating using order 6 normal geodesic algorithm; middle: simulating using 5th order geodesic algorithm and subgrid technique; bottom: simulating using 5th order geodesic algorithm.
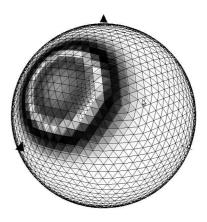
**Figure 6.** Propagation wave-forms on the earth's surface at timestep 2500 (0.075s). Subgrid fields is near the center of the figure.

**Figure 7.** Propagation wave-forms on the earth's surface at time steps 1600 (0.048 s). 18 normal grid-cells are subgridded.

propagation period of about 0.134 s (correspond to the period of EM waves travel around the Earth's sphere at light speed), which proves the correctness of our subgrid technique. Note that in the figure, the top and middle results are the average EM field in an area of about 6220 km$^2$ (order 6), however the bottom result is only the average EM field in an area of about 24900 km$^2$ (order 5). It clearly shows that the introduce of subgrid technique can results in the resolution of 6th order while using the 5th order geodesic FDTD algorithm. Figure 6 illustrates the wave propagation on the Earth's surface at timestep 2500 (0.075 s), which also proves the correctness of the subgrid technique.

Here we list a table to describe the simulation condition and computational cost of the above experiments, thus to prove the advantage of using the subgrid technique. From the table it is clear shown that to obtain the results with the same resolution, it saves much computational time and computer memory using the subgrid technique.

Another simulation example is given here to further prove the performance of the subgrid technique. In this experiment, four simulation conditions are considered: A) 4th order simulation; B) 5th order simulation; C) 4th order simulation with 1 subgrid; D) 4th order simulation with 18 subgrids. The subgrid simulation results at 1600 time steps (0.048 s) are mapped on to the sphere surface (case D) in

**Table 1.** Comparison of different simulation condition.

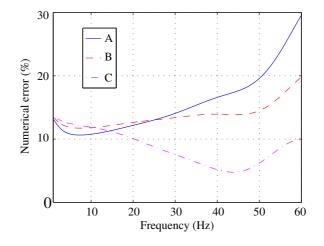| Conditions | A (Top results) | B (Middle results) | C (Bottom results) |
|---|---|---|---|
| Grid-cell no. | 81920 | 20480 | 20480 |
| Resultion | 125 km | 125 km | 250 km |
| Memory applied | 300 MB | 95 MB | 80 MB |
| Timesteps | 100000 | 100000 | 100000 |
| Simulation time | 40 min | 12 min | 12 min |



**Figure 8.** Comparison of numerical errors at different conditions: A) 4th order simulation; B) 4th order simulation with 1 subgrid (observation grid); C) 4th order simulation with 18 subgrids (including observation grid). The numerical errors are obtained by comparing these results to the 5th order simulation result.

Figure 7, which shows that the subgrids technique adapts well with the geodesic FDTD algorithm. Figure 8 compares the frequency domain numerical errors (taking case B as the reference as it is simulated using the highest resolution of the four, thus gives the most accurate results). In this figure, it is clearly seen that below 20 Hz, the numerical errors are similar to each other; in 20–60 Hz, the subgrid results give less numerical errors, thus provide more accurate results. Also the more the normal grid cells are subgridded, the more accurate the results can be obtained.

## 5. POTENTIAL APPLICATIONS OF THE SUBGRID TECHNIQUE

Figures 9 and 10 are illustrated potential applications of the subgrid technique, and Figure 9 is described a long distance system to study wave propagation between the transmitter and the receiver. In order to obtain rigorous simulation results, for positions of the transmitter and the receivers the grid-cells require resolution as high as possible. In real applications, the anomalous phenomena of VLF propagation in earthquake regions have been observed many times, previous studied only focused on model locale regions using traditional FDTD that do not include global EM noises and global EM wave propagations, and the geodesic FDTD algorithm can consider these global influence but with much unnecessary computational consume. The model structure proposed in Figure 6 can overcome the disadvantage of the geodesic FDTD algorithm, thus provides efficient solutions to the locale VLF study.
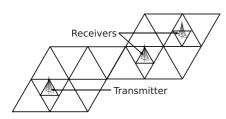


**Figure 9.** Example of subgrid application. Several normal grid-cells are subgridded.
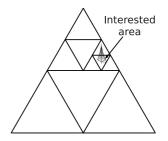
**Figure 10.** Example of subgrid application. Subgrid technique is used several times to achieve high resolution in a small area.

A high order subgrid technique is described in Figure 10. To study locale effect of global EM activities such as lightning, because the interested place is limited to a small area (sometime the area has radius of only several kilometer), and the use of subgrid technique can not provide enough resolution, thus high order subgrid technique is to be applied. In this technique, the subgrid cell can be divided again into smaller ones, namely the 2rd order subgrid cell. In order to achieve interested resolution, this procedure can be repeated again.

## 6. CONCLUSIONS AND ONGOING WORK

In this work, we have proposed a subgrid technique for the geodesic FDTD algorithm, which is applied to solve ELF EM wave propagation problems in the Earth-ionosphere system. Coupled with the subgrid technique, the global FDTD algorithm can solve EM problems in specific locale regions without unnecessary computational burden. However, the subgridding procedure will also require special treatment of border fields and complex subgrid model constructions. It is also noted that using the subgrid technology makes the stable relation of the whole geodesic FDTD algorithm stricter. At present, we are extending this work into fully 3D subgrid technique for the geodesic FDTD algorithm. This will permit real EM propagation study in locale regions of the Earth-ionosphere system.

## ACKNOWLEDGMENT

## REFERENCES

1. Simpson, J. J., "Current and future applications of 3-D global earth-ionosphere models based on the full-vector Maxwell's Equations FDTD method," *Surveys in Geophysics*, Vol. 30, 105–130, 2009.
2. Sevgi, L., F. Akleman, and L. Felsen, "Groundwave propagation modeling: Problem-matched analytical formulations and direct numerical techniques," *IEEE Antennas and Propagation Magazine*, Vol. 44, 55–75, 2002.
3. Berenger, J., "Long range propagation of lightning pulses using the FDTD method," *IEEE Transactions on Electromagnetic*, Vol. 47, 1008–1012, 2005.
4. Hu, W. and S. Cummer, "An FDTD model for low and high altitude lightning-generated EM fields," *IEEE Transactions on Antennas and Propagation*, Vol. 54, 1513–1522, 2006.
5. Soriano, A., E. Navarro, D. Paul, and J. Porti, "Finite difference time domain simulation of the Earth-ionosphere resonant cavity: Schumann resonances," *IEEE Transactions on Antennas and Propagation*, Vol. 53, 1535–1541, 2005.
6. Yang, H., V. P. Pasko, and G. Satori, "Seasonal variations of global lightning activity extracted from Schumann resonances

using a genetic algorithm method," *Journal of Geophysical Research*, Vol. 114, 1–10, 2009.

7.  Simpson, J. J. and A. Taflove, "Efficient modeling of impulsive ELF antipodal propagation about the earth sphere using an optimized two-dimensional geodesic FDTD grid," *IEEE Antennas and Wireless Propagation Letters*, Vol. 3, 215–218, 2004.

8.  Simpson, J. J. and A. Taflove, "ELF radar system proposed for localized D-region ionospheric anomalies," *IEEE Geoscience and Remote Sensing Letters*, Vol. 3, 500–503, 2006.

9.  Simpson, J. J., R. Heikes, and A. Taflove, "FDTD modeling of a novel ELF radar for major oil deposits using a three-dimensional geodesic grid of the earth-ionosphere waveguide," *IEEE Transactions on Antennas and Propagation*, Vol. 54, 1734–1741, 2006.

10. Holland, R., "THREDS: A finite-difference time-domain EMP code in 3D spherical coordinates," *IEEE Transactions on Nuclear Science*, Vol. 30, 4592–4595, 1983.

11. Simpson, J. J., "Electrokinetic effect of the Loma Prieta earthquake calculated by an entire-earth FDTD solution of Maxwell's equations," *Geophysical Research Letters*, Vol. 32, 1–4, 2005.

12. Simpson, J. J. and A. Taflove, "Two-dimensional FDTD model of antipodal ELF propagation and Schumann resonance of the Earth," *IEEE Antennas and Wireless Propagation Letters*, Vol. 1, 53–56, 2002.

13. Bannister, P., "ELF propagation update," *IEEE Journal of Oceanic Engineering*, Vol. 9, 179–188, 1984.

14. Wang, Y., H. Xia, and Q. Cao, "Analysis of ELF attenuation rate using the geodesic FDTD algorithm," *2010 International Conference on Microwave and Millimeter Wave Technology*, 1413–1415, 2010.

15. Taflove, A. and S. C. Hagness, *Computational Electrodynamics: The Finite-Difference Time-Domain Method*, Artech House, 2005.

16. Xia, H., Y. Wang, and Q. Cao, "Local high-resolution technique in FDTD modeling of ELF propagation in the earth ionosphere cavity," *IEEE Antennas and Wireless Propagation Letters*, Vol. 9, 649–652, 2010.

17. Wang, Y., H. Xia, and Q. Cao, "Analysis of ELF propagation along the earth surface using the FDTD model based on the spherical triangle meshing," *IEEE Antennas and Wireless Propagation Letters*, Vol. 8, 1017–1020, 2009.